

# Rapid Detection of High-impedance Arc Faults in Medium Voltage Electrical Distribution Systems

Kriti Thakur<sup>a,b</sup>, Divyanshi Dwivedi<sup>a,e</sup>, K. Victor Sam Moses Babu<sup>a,b</sup>, Alivelu Manga Parimi<sup>b</sup>, Prasanta K. Panigrahi<sup>c,d</sup>, Pradeep Kumar Yemula<sup>e</sup>, Pratyush Chakraborty<sup>b</sup>, Mayukha Pal<sup>a,\*</sup>

<sup>a</sup>*ABB Ability Innovation Center, Asea Brown Boveri Company, Hyderabad, 500084, Telangana, India.*

<sup>b</sup>*Department of Electrical and Electronics Engineering, Birla Institute of Technology and Science, Pilani- Hyderabad Campus, Hyderabad, 500078, Telangana, India.*

<sup>c</sup>*Department of Physical Sciences, Indian Institute of Science Education and Research, Kolkata, Mohanpur, Nadia, 741246, West Bengal, India.*

<sup>d</sup>*Centre for Quantum Science and Technology, Siksha 'O' Anusandhan university, Bhubaneswar, 751030, Odisha, India.*

<sup>e</sup>*Department of Electrical Engineering, Indian Institute of Technology, Hyderabad, 502205, Telangana, India.*

---

## Abstract

High-impedance arc faults in AC power systems have the potential to lead to catastrophic accidents. However, significant challenges exist in identifying these faults because of the much weaker characteristics and variety when grounded with different surfaces. Addressing a noteworthy gap in prior research, which largely focused on arc fault detection in low-voltage systems. A novel approach has been applied that offers rapid arc fault detection for medium voltage distribution lines. In contrast to existing black-box feature-based approaches, Hankel alternative view of the Koopman (HAVOK) analysis developed from nonlinear dynamics has been applied which offers not only interpretable features but also opens up new application options in the area of arc fault detection. The method displays a much faster detection speed within 0.45 ms making it appropriate for real-time applications. It demonstrates the ability to detect arc faults across various scenarios, boosting its practical importance for stakeholders in safety-critical industries.

---

\*Corresponding author

Email address: [mayukha.pal@in.abb.com](mailto:mayukha.pal@in.abb.com) (Mayukha Pal)

*Keywords:* Arc fault detection, electrical distribution system, High impedance arc faults, Hankel alternative view of the Koopman, Power System Safety.

---

## 1. Introduction

The International Energy Agency (IEA) reports a worldwide electricity consumption rise of about 6% during 2021 , with an average yearly growth of 2.7% projected from 2022 to 2024 [1]. The growing power demand has resulted in a growing number of safety hazards. Therefore, it is crucial to protect the electrical distribution system [2, 3]. The predominant fault type in the distribution network is the single-phase grounding fault, which constitutes around 80% of the overall fault occurrences. A high impedance fault (HIF) is a frequently occurring form of single-phase grounding fault. It is characterized by a wire coming into contact with a surface made of a material with high impedance [4]. The HIF process frequently produces an arc, which is followed by the emission of heat as well as light. Therefore, it is often referred to as a high-impedance arc fault (HIAF) [5]. With the integration of multiple energy sources into the power grid ,the operating environment becomes more complicated and unpredictable, further increasing the likelihood of HIAF events [6].

An arcing fault is a particular type of fault that occurs in medium voltage (MV) distribution lines [7]. This fault has the ability to create a shock danger, induce equipment failure, and start a catastrophic fire. Detecting an arcing fault in distribution lines is particularly tough because of its short duration. Thus, to guarantee electrical safety, it's critical to precisely identify arc faults. However, because of their features, particularly their great unpredictability and strong concealment, it is difficult to discover arc faults in real-world engineering applications.

The occurrence of an arc is directly associated with various types of faults in MV distribution lines[7]. It is usually accepted that an incipient fault includes an arc, particularly an incipient fault in an underground cable [8]. The magnitude of the electric current in these arcing faults could reach several kilo-amperes,

making them known as high-current arcing faults. Furthermore, the occurrence of a HIF is consistently associated with an arc, wherein the current of the fault typically ranges from just a few tens of amperes [9]. This type of defect is commonly known as a low current arcing fault.

Researchers worldwide have undertaken substantial investigations on the detection of arc faults that mostly concentrated on identifying arc faults in low-voltage systems [10]. Investigations have been conducted to differentiate between AC and DC configurations in the field of low-voltage systems. However, it is crucial to highlight the insufficient attention given to medium voltage systems in the current literature.

Presently, there exist two basic strategies for the detection of arc faults: traditional approaches [11, 12] and those based on artificial intelligence (AI) [13]. The principal techniques for detecting arc faults involve the analysis of the time domain [11], frequency domain[14], time-frequency domain [15], or the observation of physical phenomena such as sound, light, or electromagnetic radiation. In the past few years, there has been a developing interest in the application of AI in the field of arc fault detection. Numerous AI strategies have been utilized for the goal of identifying arc faults, revealing a varied range of techniques within this field. Within AI methodologies, arc fault detection is classified into two different categories: techniques based on machine learning and neural network-based techniques [13].

In [12], current profiles are examined utilizing Fast Fourier Transform (FFT), and detectors are engineered to focus on the third, fifth, and seventh harmonic components. This approach utilises two criteria to identify and indicate the occurrence of HIAF. An Empirical Mode Decomposition (EMD)-based method is employed for the detection and classification of high-impedance arc faults through the analysis of arc voltage data. In conjunction with EMD, machine learning methods such Artificial Neural Networks (ANN), Support Vector Machines (SVM), and k-Nearest Neighbours (KNN) are utilised. The arc signals undergo processing using EMD to derive Intrinsic Mode Functions (IMFs), which subsequently serve as inputs for the machine learning models utilised

in categorisation[16]. An approach for detecting arc fault is proposed that includes SVM, enhanced multi-scale fuzzy entropy (IMFE), and variational mode decomposition (VMD) approaches [17].

Nevertheless, the classic approaches are confronted with the challenges of excessive computational complexity and poor generalization ability when applying the Fast Fourier transform (FFT), Discrete Wavelet Transform (DWT), and similar algorithms for rapid calculations. These approaches offer detection using simple circuits and algorithms, however they are subject to switching noise and load change. In complex power generation and distribution systems, wherein many loads operate at the same time, the chance of arcing in a branch is relatively great. However, it is impractical to place arc fault detection equipment in each branch. Consequently, extracting arc fault features related to the main circuit current presents a major obstacle in the domain of arc fault identification. Studies on the application of machine learning to address the issue of arc fault detection are represented in the target identification of fault features [18] or by building up a classification model to differentiate fault features. Basic classification models include the clustering method and mapping algorithm. These algorithms are less resilient on isolated points and highly disturbed data [19]. The problem of sensitivity to hyperparameter choice bears enormous significance. Machine learning faces a significant problem concerning the potential overfitting of algorithms to the training data [20]. Comprehending these limitations is crucial for stakeholders in safety-critical industries, as it guides the development and application of dependable and effective arc fault detection methods.

In the past few years, the Koopman operator [21] has been utilized in a wide variety of nonlinear time series analysis and has achieved significant success. A notable approach for the investigation of nonlinear dynamical systems is the HAVOK analysis [22]. HAVOK analysis was proposed by Brunton [22]. It uses the delay embedding approach and the Koopman theory [23] to reduce chaotic dynamics into a linear model with intermittent forcing.

The HAVOK technique has been widely implemented across numerous fields,

displaying its versatility in electrical engineering [24], and physics[25]. In [24], the HAVOK method is used to analyze real-time streaming data from electrical distribution networks' distribution-level phasor measurement units. Time series data from behavioral and psychological research[26] can have substantial non-linear components, making analysis challenging. To address these difficulties, HAVOK analysis is applied as a flexible framework for capturing and analysing underlying dynamics. By offering a linear framework, recreating attractor manifolds, and estimating the amount of nonlinear forcing in the dynamic system, it makes a more complex analysis possible. The significant contributions of this research include:

1. This study involves the implementation of a physics-informed HAVOK method for high-impedance arc fault detection, resulting in a detection time that is 50% faster than the methods available in the literature.
2. The technique successfully differentiates arc faults from other disturbances in medium voltage distribution lines, achieving an accuracy of 100%, ensuring precise and reliable arc fault identification.
3. By providing rapid detection of arc faults within 0.45 ms, the approach enhances the protective mechanisms of electrical distribution networks, potentially preventing major faults and damage.

This article has been arranged as follows. Section 2 discusses the development of the arc model in PSCAD software and generating data for a medium voltage distribution system. Section 3 discusses the approach utilized for arc fault detection. Section 4 presents the experimental scenarios are used to validate the effectiveness of the suggested detection algorithm. Section 5 offers an analysis of our proposed method compared to existing approaches presented in the literature. Section 6 gives the conclusion.

## **2. Arc Modelling**

A Medium-voltage distribution system has been considered that operates at 12 kV and 50 Hz. The simulation was performed in PSCAD software. The sys-

tem consists of three buses labeled as B1, B2, and B3, and two loads of 10 MW each shown in Figure 1. An arc model has been integrated into the system to precisely replicate arc faults. A HIAF model is commonly created by connecting a variable resistor,  $R_{arc}$ , to represent the arc, and a constant resistor to indicate the poor conductivity of the grounding material,  $R_T$  as shown in Figure 2 [7]. Typically, the nonlinear aspects of the arcing process could be represented by  $R_{arc}$ , and the current amplitude magnitudes are obtained by modifying  $R_T$ . The  $R_T$  value impacts the amount of current that can flow through the circuit during an arc fault. A greater  $R_T$  value often results in reduced current flow, which can influence the detecting capabilities of the system. The sensitivity of the detection system to discover arc faults can be modified by the  $R_T$  value. In simulations, modifying the  $R_T$  helps to explore how varying resistance levels affect the system's response to arc faults. This helps in improving detection method and analysing the dynamics of arc faults.

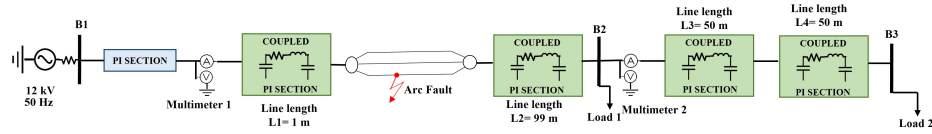


Figure 1: Model for the MV distribution system that includes an arc fault.

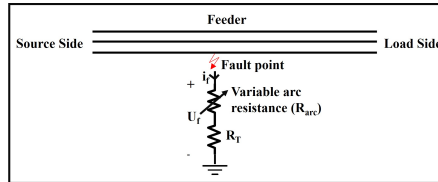


Figure 2: Standard structure of a HIAF model.

The heat balance equation is typically used to determine  $R_{arc}$  for black-box models [27].

$$\frac{dQ}{dt} = u \cdot i - P \quad (1)$$

where  $P$  (MW) denotes the dissipated power,  $Q$  (MW·s = MJ) denotes the energy that is preserved in the arc, and  $i$  (kA), and  $u$  (kV) denote the arc current and voltage, respectively. Equation (1) could be subsequently rewritten as:

$$\frac{dQ}{dg} \cdot \frac{dg}{dt} = P \left( \frac{u \cdot i}{P} - 1 \right) \quad (2)$$

$$\frac{1}{g} \frac{dg}{dt} = \frac{1}{g \cdot P^{-1} \cdot \left( \frac{dQ}{dg} \right)} \left( \frac{u \cdot i}{P} - 1 \right) \quad (3)$$

where the arc conductance is denoted by  $g$  ( $\Omega^{-1}$ ). Using the expression  $g \cdot P^{-1} \cdot \left( \frac{dQ}{dg} \right) = T$ , the Mayr model, a widely recognized type of black-box model, could be defined as follows:

$$\frac{ln g}{dt} = \frac{1}{T} \left( \frac{u \cdot i}{P} - 1 \right) = \frac{1}{T'} (u \cdot i - P) \quad (4)$$

where  $T$  is expressed in unit of seconds (s) and  $T' = T \cdot P$ . Several formulas can be used to define the arc parameters  $T'$ ,  $T$  and  $P$  depending on the arcing process hypothesis that is used. It has been proven that there is more than one relationship between the arc parameter specifications and the arc characteristics that are presented [28]. The fundamental source of current distortion is the nonlinearity of  $R_{arc}$ , the arc resistance. This nonlinearity directly influences the system's behavior and can be expressed mathematically as given in 4:

$$R_{arc} = \frac{1}{g} = e^{\int \frac{1}{T'} (u \cdot i - P) dt} \quad (5)$$

Therefore  $T'$  and the difference between  $P$  and  $u \cdot i$  have an impact on  $R_{arc}$ . This difference is known as residual power, and it represents the energy-storing capacity of an arc.

The nonlinear nature of arc faults could be changed by three fundamental arc characteristics, each providing a distinct physical interpretation and a means for effectively modifying arc resistance. These characteristics play a key role in determining and characterizing residual power. Consequently, they enable the regulation of three components of current distortions, hence boosting simulation

accuracy. Ideally, an ideal current distortion should be nearly centered around the zero point and exhibit symmetry. However, in practical settings, distortion offsets occur relative to higher or lower zero points due to variations in the lag between the dissipated power of the arcs and the energizing power. Consequently, the three primary variables in the current waveforms, as illustrated in Figure 3, are the duration, extent, and offset of distortions. Figure 3 includes additional labels to visually depict the three features in a more understandable manner.

1. DURATION: The term “duration” describes the period of time of the zero-off interval (ZOI), which is a component of the total distorted interval (DI), allowing models to precisely reflect how long the arc resistance remains at a crucial value, which affects the current waveform. The ZOI waveform aligns with the x-axis when the arc resistance reaches a particular value.
2. EXTENT: The slope of the line between the ZOI’s beginning and finishing points is known as the extent. It indicates the rate of change of current during the fault event, which is essential for distinguishing arc faults from other fault types.
3. OFFSET: The offset is the separation that exists between the zero-crossing point and the midpoint of DI. It indicates any shifts in the waveform because of the arc fault.

By effectively managing these characteristics, the simulations produce waveforms that closely resemble actual system behavior, leading to improved detection capabilities, a deeper understanding of fault dynamics, and validation of detection methods.

Since dissipated power  $P$  has a direct relationship with energizing power, which is determined by  $u.i$  [29], a mathematical model of  $P$  can be constructed as follows:

$$P = F(ui) = u.i + P_{res}(t) \quad (6)$$

$P_{res}(t)$  is the residual power function in this case, after which arc resistance

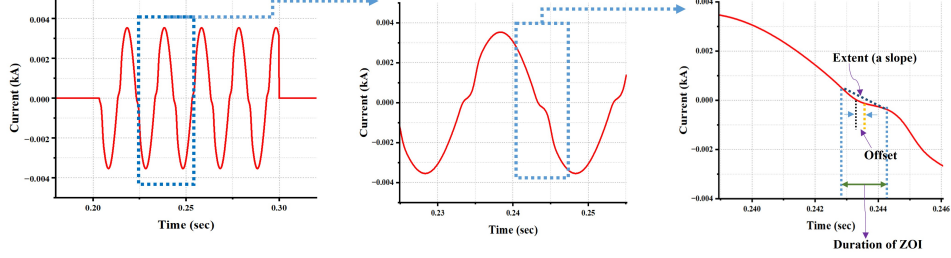


Figure 3: The waveforms of arc current observed in the 12 kV distribution system field.

$R_{arc}$  in (5) could be formulated as follows.

$$R_{arc} = e \int \frac{1}{T} P_{res}(t) dt \quad (7)$$

The residual power could be regulated through the utilization of three current features: Duration, Extent, and Offset. This equation facilitates the adjustment of  $R_{arc}$  throughout the entire simulation period, thereby enabling the generation of waveforms depicting current with an arc fault. Suppose  $t_m$  denotes the time at which  $R_{arc}$  initially achieves its maximum value in a half cycle; at that time, the residual power is indicated as  $P_{res}(t_m)$ . According to the characteristics demonstrated by the standard models,  $P_{res}^{(t_m)}(t)$  could be expressed as a periodically segmented linear function:

$$P_{res}^{(t_m)}(t) = \begin{cases} a_1 \left( t - t_m - \frac{\text{DURATION}}{2} \right) - b_1, & t \in \left[ t_m - \frac{\text{DURATION}}{2}, t_m + \frac{\text{DURATION}}{2} \right) \\ a_2 \left( t - t_m - \frac{\text{DURATION}}{2} \right) - b_2, & t \in \left[ t_m + \frac{\text{DURATION}}{2}, t_m + \frac{\text{Time}}{2} - \frac{\text{DURATION}}{2} \right) \end{cases} \quad (8)$$

where

$$a_1 = \frac{-8 \ln \text{EXTENT}}{\text{DURATION}^2}, \quad b_1 = \frac{4 \ln \text{EXTENT}}{\text{DURATION}}, \quad (9)$$

$$a_2 = m \cdot \frac{-16 \ln \text{EXTENT}}{\text{DURATION}(\text{Time} - 2\text{DURATION})}, \quad b_2 = m \cdot b_1$$

$m$  is a coefficient and  $\text{Time}$  indicates the amount of time of an interval (20 ms in a 50 Hz system).

OFFSET is to control the distortion offset. The moment at which the maximum arc resistance occurs  $t_m$  is controlled by OFFSET and satisfies:

$$\begin{cases} |u_f(t_m)| = \text{OFFSET}, \\ \text{sgn}(\text{OFFSET}) \cdot \frac{d|u_f(t_m)|}{dt} \geq 0 \end{cases} \quad (10)$$

where  $u_f$  (kV) indicates the voltage of the fault. EXTENT: Distortion extent is determined by the amount of the maximum resistance, i.e.,  $R_{\text{arc}}(t_m)$ . it is calculated as:

$$R_{\text{arc}}(t_m) = R_{\text{arc},0} + e^{\int_{t_0}^{t_m} P_{\text{res}}(t) dt} \quad (11)$$

where,  $R_{\text{arc},0} = R_{\text{arc}}(t_0)$ , and indicates the minimal resistance during  $[t_m - \text{Time}/2, t_m]$ .  $R_{\text{arc},0}$  is the resistance when an arc is highly conductive and which could be ignored in comparison to the huge grounding resistance  $R_T$ . Thus, put  $R_{\text{arc},0} = 1$  and 14 represent as:

$$\begin{aligned} \ln R_{\text{arc}}(t_m) &= \int_{t_0}^{t_m - \text{DURATION}/2} P_{\text{res}}(t) dt + \int_{t_m - \text{DURATION}/2}^{t_m} P_{\text{res}}(t) dt \quad (12) \\ &= \left( \frac{\text{Time}}{8} - \frac{\text{DURATION}}{4} \right) \cdot m \cdot b_1 + \frac{1}{2} \cdot \frac{\text{DURATION}}{2} \cdot b_1 \\ &= \left( \frac{\text{Time}}{8} - \frac{\text{DURATION}}{4} \right) \cdot m \cdot b_1 + \ln \text{EXTENT} \end{aligned}$$

Hence from the equation above, the maximum resistance that arises at  $t_m$  can be individually reflected by EXTENT if  $m$  is taken as 0.

DURATION: Distortion duration is determined by the length of ZOI, which is exactly equal to DURATION. Hence the distorted duration also becomes individually controlled. As a result, independent control of all three arc characteristics theoretically make it more flexible in controlling distortion characteristics and achieving the different waveforms. In summary, the modelling of an arc fault entails a systematic process starting with the identification of the

time instance  $t_m$  via the OFFSET parameter, which indicates the initial appearance of arc fault characteristics. Utilising this  $t_m$ , the residual power  $P_{\text{res}}(t_m)$  is computed based on DURATION and EXTENT, capturing the temporal and magnitude aspect of the arc fault. The residual power is utilised to calculate the arc resistance  $R_{\text{arc}}$ , so establishing a correlation between power dissipation and resistance during the fault. Ultimately, by regulating  $R_{\text{arc}}$ , arc current waveforms are generated, enabling a realistic simulation of arc faults for analysis and validation. The arc modelling is given in Figure 4.

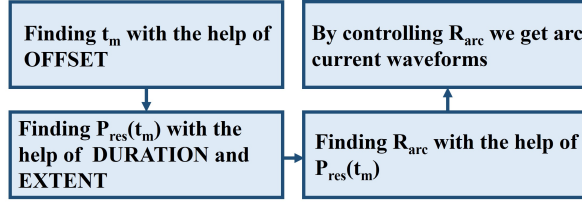


Figure 4: Modelling of an arc fault.

### 3. Method

The suggested approach is well-suited for examining the dynamic response and showing the nonlinear properties inherent in the electrical distribution system. To illustrate this, take a continuous-time dynamical system with a state vector  $y(t)$ ,

$$\frac{d}{dt}y(t) = f(y(t)) \quad (13)$$

The variable  $y(t) \in \mathbb{R}^n$  reflects the state of the system at time  $t$ . The function  $f$  describes the dynamics of the state variable  $y$ . Equation 13 depicts a continuous-time dynamical system evolving over time. The updated formula for the discrete-time acquisition of state samples from current data is written as [30].

$$y_{k+1} = F(y_k) = y_k + \int_{k\Delta t}^{(k+1)\Delta t} f(y(\tau))d\tau \quad (14)$$

In the provided expression, the term  $y_k = y(k\Delta t)$  indicates the sampled point of the system's trajectory generated from equation (14), where  $k$  is an integer index and  $\Delta t$  signifies the time interval between consecutive samples. The symbol  $F$  denotes a discrete-time propagator. The variable  $\tau$  denotes the integration variable in the integral representation of the system dynamics. This describes the evolution of the system state during a discrete time step  $\Delta t$ , incorporating the impacts of the function  $f(y(\tau))$ , which characterizes the system's dynamics during that period.

### 3.1. Arc Fault Detection using Hankel Alternative View of Koopman Analysis

The delay embedding approach is utilized to reconstruct the state space of a dynamical system from a time series. The basic concept is to produce a multi-dimensional representation of the time series data, which represents the temporal dependencies and dynamics of the system. In our work of arc fault detection, the time-series current data  $i(t)$  taken from system Figure 1, the time shifted measurement of  $i(t)$  is utilized and stack them to generate the Hankel matrix  $\mathbb{H}_m$ , as explained in [31]. Subsequently, eigen time delay coordinates are acquired using the method of singular value decomposition (SVD) applied to the Hankel matrix  $\mathbb{H}_m$ .

$$\mathbb{H}_m = \begin{bmatrix} i(t_1) & i(t_2) & \dots & i(t_p) \\ i(t_2) & i(t_3) & \dots & i(t_{p+1}) \\ \vdots & \vdots & \ddots & \vdots \\ i(t_q) & i(t_{q+1}) & \dots & i(t_T) \end{bmatrix} \quad (15)$$

In the preceding expression, the time points  $t_{j+1} = t_j + \tau$  (where  $j = 1, \dots, T - 1$ ),  $q$  signifies the number of points in the trajectory, and  $p$  represents the window length, representing the largest periodicity obtained by the Hankel matrix.

Following the application of SVD, the SVD of a matrix  $\mathbb{H}_m$  is the process of decomposing  $\mathbb{H}_m$  into the multiplication of three matrices  $U\Sigma V^T$ , where the columns of  $U$  and  $V$  are orthogonal and normalized, and  $\Sigma$  is a diagonal matrix

with positive real values. The resulting matrix is the product of these three components.

$$\mathbb{H}_m = U\Sigma V^T \quad (16)$$

where  $U \in \mathbb{R}^{n \times n}$ ,  $\Sigma \in \mathbb{R}^{n \times m}$ ,  $V \in \mathbb{R}^{m \times m}$ .

The SVD arranges the columns of  $U$  and  $V$  in a hierarchical order based on their ability to best represent the columns and rows of the matrix  $\mathbb{H}_m$ , respectively. In general,  $\mathbb{H}_m$  gains a low-rank approximation for the first  $r$  columns of  $U$  and  $V$ , which is invariant to the Koopman variant for the states. Eigen time series in  $U$  provides a Koopman invariant measurement system on the attractor. Koopman theory presents a structure for evaluating non-linear dynamical systems using linear approaches. In the proposed methodology, the operation of SVD on the Hankel matrix  $\mathbb{H}_m$  reveals that all columns of  $\mathbb{H}_m$  are approximately numerically dependent on the leading  $r$  columns of  $U$ , signifying the presence of a measurement subspace. Thus, the eigen time-delay coordinates in  $U$  constitute this measurement subspace.

When the Koopman operator acts on any of these measurement coordinates, the resultant representation remains within the same subspace, as all columns of  $\mathbb{H}_m$  are spanned by the columns of  $U$ . This insight results in the development of a data-driven Koopman invariant measuring system, expressed using time-delay coordinates obtained from the Hankel matrix.  $\mathbb{H}_m$  could be expressed by iterates of the Koopman operator as  $i(t_2) = \mathbb{K}i(t_1)$ . Koopman operator operates on all measurements of our states. So, every element of the Hankel matrix can be described in terms of the Koopman operator applied many times to the initial condition  $i(t_1)$ . Therefore, we could alternatively rewrite the Hankel matrix as [31]:

$$\mathbb{H}_m = \begin{bmatrix} i(t_1) & \mathbb{K}i(t_1) & \dots & \mathbb{K}^{p-1}i(t_1) \\ \mathbb{K}i(t_1) & \mathbb{K}^2i(t_1) & \dots & \mathbb{K}^pi(t_1) \\ \vdots & \vdots & \ddots & \vdots \\ \mathbb{K}^{q-1}i(t_1) & \mathbb{K}^qi(t_1) & \dots & \mathbb{K}^{T-1}i(t_1) \end{bmatrix} \quad (17)$$

The columns of equation 16, and hence equation 17, are efficiently approximated by the first  $r$  columns of  $U$ , making these eigen-time-series a Koopman-invariant measurement system. At the same time, the first  $r$  columns of  $V$  constitute a time series that captures the magnitude of each column of  $U\Sigma$  within the data. A plot of matrix  $V$ 's first three columns yields an embedded attractor. Then we identify the optimum singular value hard threshold coefficient and computed  $r$ . Then the time history of  $V$  components are taken and build a regression model on those eigen time delay coordinates. A linear time series that substantially mirrors the input time series is produced by the initial  $(r - 1)$  variables of  $V$  that gives a very nice regression fit. Rather than developing a closed linear model for the initial  $r$  variables in  $V$ , a linear model is established based on the first  $(r - 1)$  variables and the last variable  $v_r$  gives a bad regression fit which will function as a forcing term.

$$\frac{d}{dt}\mathbf{v}(t) = \mathbf{A}\mathbf{v}(t) + \mathbf{B}\mathbf{v}_r(t). \quad (18)$$

Here  $\mathbf{v} = [v_1 \ v_2 \ \dots \ v_{r-1}]^T$  is a vector of the first  $r - 1$  eigen-time-delay coordinates.  $v_r$  serves as an input forcing that influences the linear dynamics in 18, resulting in the nonlinear dynamics in ???. Whenever a nonlinearity exists in the system, it undergoes a bursting phenomenon, which serves as an intermittent forcing signature that is forcing operator. The matrix  $\mathbf{A}$  defines the linear dynamics of the system. It defines the evolution of  $\mathbf{v}(t)$  without external influences. The matrix  $\mathbf{B}$  serves as a connection between  $\mathbf{v}(t)$  and the external force  $v_r(t)$ . It describes how the external input (forcing) impacts the evolution of the state.

The forcing operator captures the current fluctuations during arc faults. Upon initiating an arc, it produces unique electrical signatures characterized by

abrupt fluctuations in current intensity and high-frequency noise. The presence of an arc fault is indicated by the emergence of these intermittent forcing bursts, detected using the Forcing Operator. The operator enables the detection of these deviations from the norm. Finally, the forcing operator reflecting the nonlinear characteristics of the arc fault in the current data is provided by the  $r^{th}$  column. The forcing operator is the last eigentime delay coordinate that is the  $r^{th}$  column produced from the SVD of the Hankel matrix, representing the external driving force influencing the system. It captures external influences on the system, such as faults or disturbances, which are different from the natural dynamics of the system. By setting a threshold on the forcing operator, arc faults could be efficiently detected. Figure 5 provides an overview of the framework proposed in this study.

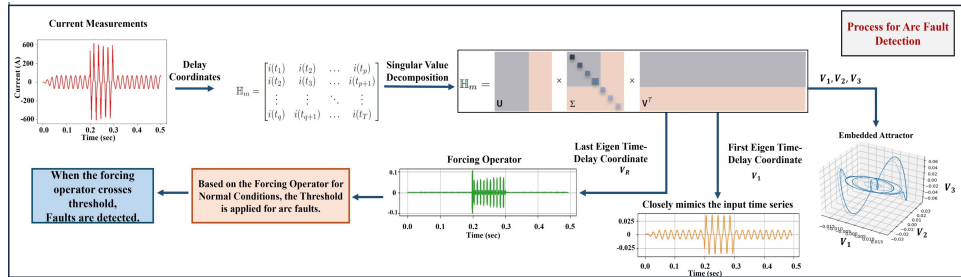


Figure 5: An overview of the suggested arc fault detection technique; HAVOK analysis framework is utilized for arc fault detection in current measurements. Time shifted current measurement is stacked into a Hankel matrix. Its singular value decomposition provides a hierarchy of eigen time series that collectively form a delay-embedded attractor. A best-fit linear regression model is then generated for the delay coordinates  $V$ ; the linear fit is excellent for the first  $r - 1$  variables, however, the last coordinate  $V_r$  is not adequately captured by a linear model. Instead,  $V_r(t)$  functions as a stochastic forcing input to the first  $r - 1$  delay coordinates, with few yet significant forcing events corresponding to sudden fluctuations in dynamics that indicate the onset of an arc fault, similar to lobe switching in chaotic systems.

Arc faults introduce nonlinear dynamics into the electrical system, which can be tough to detect using typical linear methods. The forcing operator helps to capture these nonlinear interactions by modeling how the system reacts to external influence (the arc fault). The presence of an arc fault can be consid-

ered as an intermittent driving force that changes the system’s dynamics. By studying the system’s response to these driving elements, the HAVOK approach can discover patterns that indicate the presence of arc faults.

#### 4. Results and Discussion

The following section provides the findings from the cases conducted to evaluate the effectiveness of the arc fault detection framework. The analysis employs the system illustrated in 1. The simulation integrates an arc model derived from [19], which serves as a fundamental reference for the construction and use of the model in the study. In our study, arc faults were strategically placed at different locations between Bus 1 and Bus 2, as well as between Bus 2 and Bus 3, within the medium voltage distribution system. This placement was done to examine the detection performance across different regions of the network. Altering the fault locations offered an evaluation of the robustness and precision of the arc fault detection system in recognising faults at different points along the distribution line. This approach ensures a full evaluation of the detection system over a range of possible fault conditions.

All the studies have included the data containing both arc fault and normal current waveforms. As demonstrated in the arc model, variations in the model’s variable aspects, particularly DURATION, EXTENT, and OFFSET, result in unique waveforms. The values were set based on an existing reference for a 50 Hz system with a phase-voltage level of 12 kV (the maximum voltage) for our system. The parameter ranges are as follows: OFFSET  $\in (-12, 12)$  kV, EXTENT  $\in (0, +\infty)$  k $\Omega$ , DURATION  $\in (0, 20)$  ms, which align with typical fault current behavior in medium voltage systems [19]. The selected values guarantee that the arc fault current graph aligns accurately with the graphs presented in [19], with the specific values utilised in each case detailed in Table 1 for reference.

The time series data of the current is obtained from PSCAD simulations. The HAVOK analysis is utilized to calculate eigen time delay coordinates from

the time series data. The time-delay coordinates are utilized to transform the time-series measurements into the Hankel matrix. Next, singular value decomposition was carried out to extract the columns of  $U$  and  $V$  in a hierarchical way based on their capacity to represent the columns and rows of the Hankel matrix. Subsequently, the  $V$  values were employed to formulate the linear model and forcing operator for unusual occurrences. The forcing operator facilitates comprehension of how external inputs impact the behavior of the system. Through the identification and investigation of the forcing operator, useful insights have been gained into how various inputs or perturbations affect the observed behavior. These insights are then utilised by applying the range of the forcing operator to detect arc faults using this method. Numerous experiments were conducted, and a threshold was applied to differentiate between various fault types. For arc faults, the range of the forcing operator was measured as  $+0.06$  to  $+0.18$  and  $-0.06$  to  $-0.18$ . In the case of non-arcing disturbances, the range is  $+0.045$  to  $-0.045$ . For other types of faults, the forcing operator exhibited a much broader range of  $+0.2$  and higher values and  $-0.2$  and lower values. The simulation runs for 0.5 seconds, with the fault imposed at 0.2 seconds, and remains for 0.1 seconds. The different simulation circumstances are taken into account for analysis.

#### *4.1. Case A: Low Current Arcing Fault Present*

In this scenario, the  $R_T$  value is increased. Low-current arcing faults generally arise in overhead lines, and for this fault class,  $R_T$  is non-zero. A designated current range for low-current arcing faults is employed, along with the correlation between arc voltage and current as outlined in [32]. Our simulation produces many low-current arcing faults, with parameter values over the whole designated range. Upon executing a simulation for 0.5 seconds with the introduction of an arc fault at 0.2 seconds, the resultant forcing operator deviation is noticed at 0.20045 seconds. This suggests that the system could identify the arc fault within a surprisingly short interval of 0.45 milliseconds. The value of the forcing operator in this particular case is  $-0.1035$ , suggesting a very low

magnitude and falling within the threshold range for arc faults. This case is depicted in Figure6.

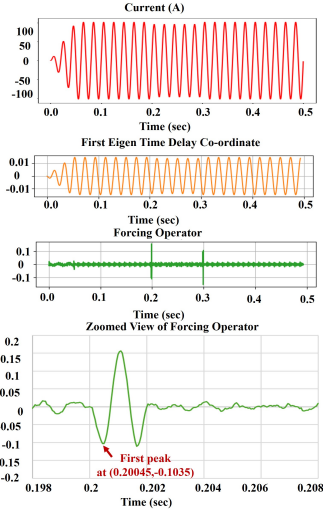


Figure 6: Low current Arcing fault with  $R_T = 1000 \Omega$ .

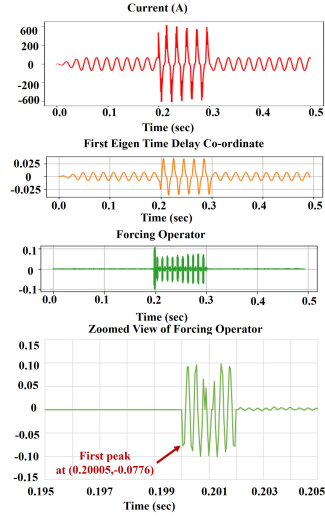


Figure 7: High current Arcing fault with  $R_T = 0.001 \Omega$ .

#### 4.2. Case B: High Current Arcing Fault Present

High-current arcing faults in MV distribution systems generally arise in underground cables that have low fault resistance. For these fault types, the  $R_T$  value is reduced to its minimum. Our simulation produces an extensive range of high-current arcing faults, guaranteeing that the parameter values encompass the complete spectrum [33]. In this circumstance, the  $R_T$  value is incredibly small. Upon conducting the simulation for 0.5 seconds and adding an arc fault at 0.2 seconds, the detection of the forcing operator deviation happens at 0.20005 seconds, confirming the system's capabilities to recognize the arc fault within a quick 0.05 milliseconds. The observed value of the forcing operator in this particular case is -0.0776675 reflecting a low value. The scenario is shown in Figure 7.

#### 4.3. Case C: Arcing Fault Present when grounded in wet cement

In practical HIAFs, fault current distortions are greatly affected by multiple parameters, especially surface humidity conditions [34]. This study investigates HIAF under conditions when it is grounded on wet cement, with DURATION set to 0.007 seconds and Extent set to 50000  $\Omega$  OFFSET set to 0.2 kV. A simulation was performed for 0.5 seconds, with the arc fault initiated at 0.2 seconds. The subsequent deviation of the forcing operator was recognized at 0.2001 seconds, proving the system's capabilities to identify the arc fault within a short interval of 0.1 milliseconds. The value of the forcing operator in this case was calculated to be 0.15201, which lies inside the threshold range for arc faults. This scenario is represented in Figure 8.

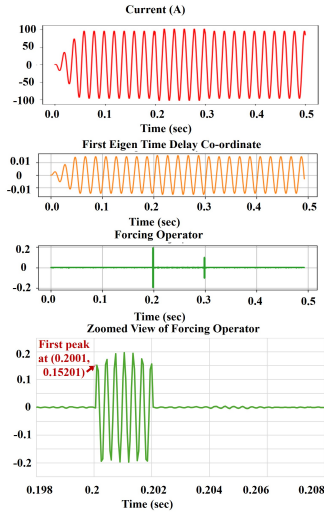


Figure 8: Arcing Fault Present when grounded in wet cement.

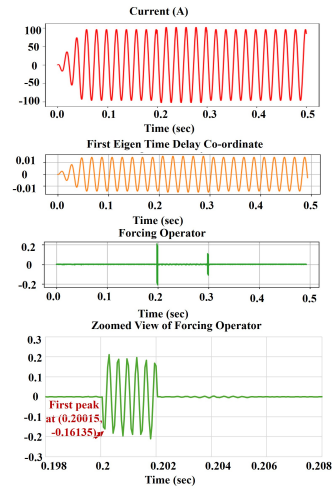


Figure 9: Arcing Fault Present when grounded in dry soil.

#### 4.4. Case D: Arcing Fault Present when grounded in Dry Soil

This study examines HIAF when it is grounded on dry soil. In this study, the DURATION is set to 0.007 seconds, the Extent is defined as 4708  $\Omega$ , and

the OFFSET is set to 0.2 kV. Simulation was conducted for 0.5 seconds, with the arc fault triggered at 0.2 seconds. The deviation of the forcing operator was identified at 0.20015 seconds, indicating the system's ability to identify the arc fault within a short interval of 0.15 milliseconds. The forcing operator's value in this instance was found to be -0.16135, which falls within the defined threshold range for arc faults. This scenario is represented in Figure 9.

#### 4.5. Case E: Nonarcing disturbance (Load Switching)

Load switching was employed to distinguish arc faults from non-arcing disturbances. The load was altered between 0.2 and 0.3 seconds, with changes in both location and load type. A variation in the forcing operator was noted at 0.2002 seconds. The forcing operator demonstrated a value of 0.04289, which falls within the range indicative of non-arcing disturbances. This situation is depicted in Figure 10.

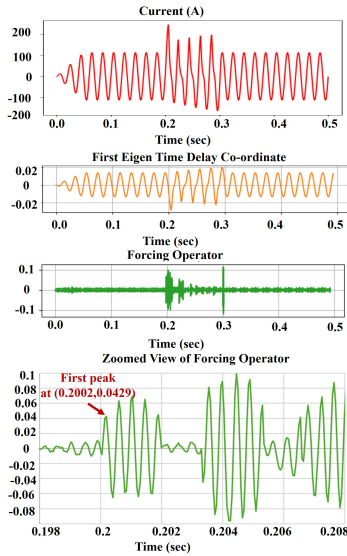


Figure 10: Non arcing disturbance (load switching).

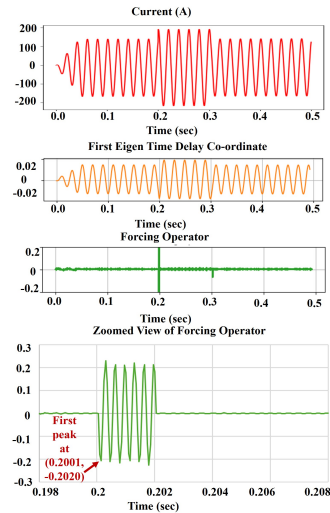


Figure 11: LG (Line-to-ground) fault without arc.

#### *4.6. Case F: LG (Line-to-Ground) fault without arc.*

In this instance, a line-to-ground fault occurs in the system, different from the arc fault scenario. The simulation runs for 0.5 seconds, with the fault introduced at 0.2 seconds and continuing for 0.1 seconds. As a result, the deviation of the forcing operator is seen at 0.2001 seconds, showing the system's ability to identify the issue within 0.1 milliseconds. The value of the forcing operator in this example is measured at -0.202. This case is shown in Figure 11.

#### *4.7. Case G: Arcing fault current with Induction Motor Load*

In this scenario, Load 1 stays constant at 10 MW, while Load 2 comprises an induction motor (IM) operating at 3.3 kV with a rated capacity of 0.2 MVA. The motor is driven through a step-down transformer, which reduces the voltage from 12 kV to 3.3 kV. The simulation runs for 0.5 seconds, with the fault introduced at 0.2 seconds and continuing for 0.1 seconds. Two scenarios have been investigated involving an IM load: one with a low-current arcing fault and the other with a high-current arcing fault. These scenarios are represented in Figures 12 and 13, respectively. In the low-current arcing fault scenario, a deviation in the forcing operator was noted at 0.20015 seconds, with the value of the forcing operator measured to be -0.08045. In the high-current arcing fault scenario, the deviation is visible at 0.2001 seconds, with the value of the forcing operator -0.08046. Both values fall within the threshold range for arc faults, confirming the robustness and effectiveness of our approach.

#### *4.8. Case H: Impact of Noise*

To evaluate the influence of measurement noise, white Gaussian noise is introduced to the current measurements. Simulations were executed with signal-to-noise ratios (SNR) of 60 dB, 70 dB, and above, during which our approach exhibited excellent performance. Incorporating white Gaussian noise at this level and higher guarantees a realistic simulation of noise that distorts the signal without substantially compromising its integrity, thus allowing an appropriate evaluation of the method's effectiveness under realistic circumstances. In cases

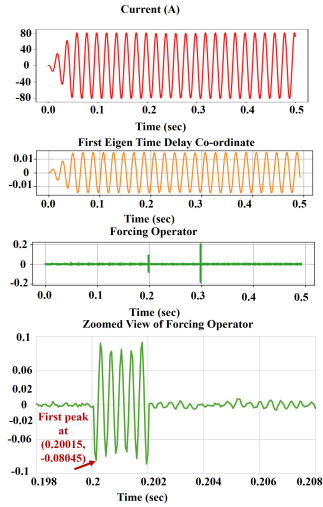


Figure 12: Low current Arcing fault with  $R_T = 1000 \Omega$  with IM load.

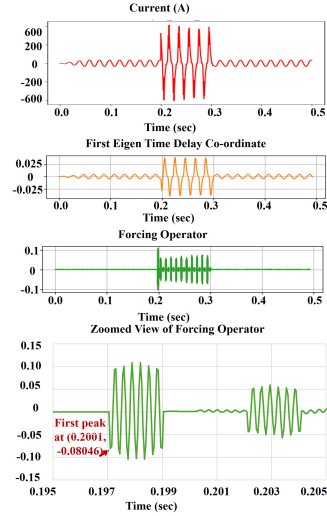


Figure 13: High current Arcing fault with  $R_T = 0.001 \Omega$  with IM load.

of extremely low signal-to-noise ratio, denoising filters may be employed for efficient noise suppression. Figure 14 depicts a scenario with a signal-to-noise ratio of 70 dB. The deviation of the forcing operator is noted at 0.20065 seconds, with a value of 0.116793459. In presence of noise, it has been found that the detection time is extended. However, the detection is still robust from the performance of our analysis.

Figure 15 displays multiple waveforms of fault current  $i_f$  for an arcing fault. By modifying the characteristics of the current—such as its extent, duration, and offset—various arc fault scenarios can be simulated, including conditions like wet soil, low-resistance earthed neutral when DURATION is set to 0.009 seconds and Extent is set to 500000  $\Omega$  OFFSET is set to 0.2 kV, dry soil, isolated neutral when DURATION is set to 0.007 seconds and Extent is set to 4708  $\Omega$  OFFSET is set to 0.2 kV, wet cement, low-resistance earthed neutral when DURATION is set to 0.007 seconds and Extent is set to 50000  $\Omega$  OFFSET is set to 0.2 kV.

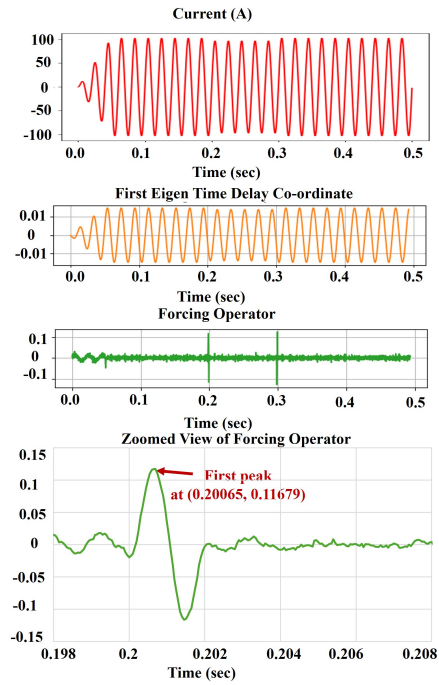


Figure 14: Low current Arcing fault with  $R_T = 1000 \Omega$  with noise.

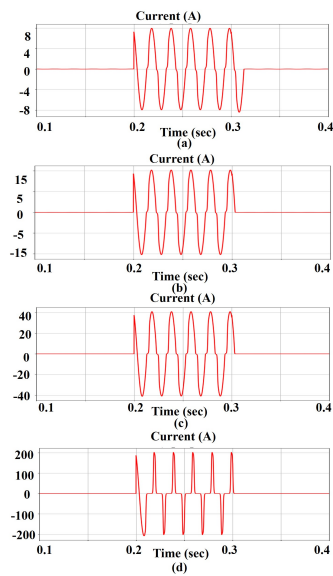


Figure 15: Arcing fault current  $i_f$  waveforms for varying distance values: (a)  $R_T = 1000 \Omega$  ( high resistance), (b)  $R_T = 500 \Omega$  (moderate resistance), (c)  $R_T = 200 \Omega$  (lower resistance), and (d)  $R_T = 50 \Omega$  (wet soil, low resistance).

Table 1: Case Study: Detection Time for Different Cases

Cases	Extent ( $\Omega$ )	Duration (seconds)	Offset (kV)	$R_T$ ( $\Omega$ )	Forcing Operator	Time of Detection (ms)
A	5000	0.00413	0.2	1000	-0.1035	0.45
B	5000	0.00413	0.2	0.001	-0.0776	0.05
C	50000	0.00700	0.2	50	0.1520	0.10
D	4708	0.00700	0.2	50	-0.1614	0.15
E	NA	NA	NA	NA	0.0429	0.20
F	NA	NA	NA	NA	-0.2020	0.10
G (a)	5000	0.00413	0.2	1000	-0.0805	0.15
G (b)	5000	0.00413	0.2	0.001	-0.0805	0.10
H	5000	0.00413	0.2	1000	0.1168	0.65

Table 1 provides an overview of the analysis of the experiments, including the corresponding time of detection for each conducted experiment. The range of the forcing operator permits the differentiation between arc faults and other types of faults, as arc faults present a lower range and require more time for detection compared to other fault types. It has been shown that a forcing operator range of +0.06 to + 0.18 and -0.06 to -0.18 helps the rapid identification of arc faults. In contrast, when the forcing operator range changes, such as +0.2 and higher values and -0.2 and lower values, the system identify other faults, while non-arcing disturbances, such as load switching, are identified with a forcing operator range of +0.045 to -0.045.

## 5. Comparison With Existing Techniques

A comparative analysis has been conducted between the proposed method and existing arcing fault detection methods found in the literature. The standard detection time for high-impedance arc faults in medium voltage networks may vary based on the specific detection methods and technologies employed. Generally, high-impedance arc faults are hard to detect because of their low fault current and stochastic nature, which can result in longer detection times compared to other fault types. Usually, detection times for high-impedance faults vary between milliseconds to several seconds. Several approaches available in the literature demonstrate varied detection times for HIFs. The Mathematical Morphology technique [35] detects HIFs in 80 milliseconds, while the Harmonic

Table 2: Comparison With Existing Techniques.

<b>Techniques</b>	<b>Detection time (ms)</b>	<b>Detection rate %</b>
Mathematical Morphology technique [35]	80	100
Harmonic Content-based method[36]	200	-
SVM and DWT based technique [37]	0.90	97.6
Proposed method	0.45	100

Content-based method[36] yields a detection time of 200 milliseconds. Additionally, the SVM and DWT based [37] technique provides a substantially faster detection time of 0.90 milliseconds. Improvements in technology continue to push for faster and more reliable detection systems in medium voltage networks. However, our proposed method demonstrates the early detection capability of arc faults. A comprehensive literature study comparing the proposed methodology with existing methodologies, demonstrating that the proposed method is 50% more faster in arc fault detection. The findings are displayed in Table 2. It is evident that the proposed method exhibits the best level of accuracy in detecting arcing faults.

## 6. Conclusion

Our research greatly contributes to the field of arc fault detection by addressing crucial gaps in existing knowledge. The application of data obtained by PSCAD simulations of medium voltage distribution lines distinguishes our analysis, filling a noteworthy gap in earlier research largely focused on low-voltage systems. The implementation of HAVOK analysis, derived from nonlinear dynamics, constitutes a shift from state-of-the-art black-box feature-based approaches. The selection not only offers interpretable features but also exposes innovative application possibilities in the context of arc fault detection.

The main achievement of the suggested technique is its capacity to identify arc faults in a minimal duration, with detection times as minimal as 0.45 ms and 0.05 ms. This rapid detection ability markedly improves the system's dependability and reaction time, mitigating the chance of damage and enhancing

the overall safety of the distribution network. Future work focuses on confirming the simulation results with real-world data. Conducting field tests would provide a more comprehensive understanding of the system's performance and potential obstacles in real applications.

The insights provided here pave the path for future developments in the domain, promoting a more secure and trustworthy operational environment.

## References

- [1] I. IEA, Electricity market report, Electron Marketpl Rep (2022).
- [2] M. Pal, A. K. Bharati, S. S. Belkhode, Nuisance trip decision management using data analytics in electrical protection system (05 2022).
- [3] M. Pal, A. K. Bharati, S. S. Belkhode, Data analytics for smart electrical protection systems (11 2021).
- [4] X. Wang, J. Gao, X. Wei, G. Song, L. Wu, J. Liu, Z. Zeng, M. Kheshti, High impedance fault detection method based on variational mode decomposition and teager–kaiser energy operators for distribution network, *IEEE Transactions on Smart Grid* 10 (6) (2019) 6041–6054.
- [5] X. Zeng, W. Gao, G. Yang, High impedance fault detection in distribution network based on s-transform and average singular entropy, *Global Energy Interconnection* 6 (1) (2023) 64–80.
- [6] S.-Y. Hyun, J.-S. Hong, S.-Y. Yun, C.-H. Kim, Y. Lee, Arc modeling and kurtosis detection of fault with arc in power distribution networks, *Applied Sciences* 12 (6) (2022) 2777.
- [7] W. Zhang, Y. Jing, X. Xiao, Model-based general arcing fault detection in medium-voltage distribution lines, *IEEE Transactions on Power Delivery* 31 (5) (2016) 2231–2241.

- [8] S. Kulkarni, S. Santoso, T. A. Short, Incipient fault location algorithm for underground cables, *IEEE transactions on smart grid* 5 (3) (2014) 1165–1174.
- [9] M. Sedighizadeh, A. Rezazadeh, N. I. Elkalashy, et al., Approaches in high impedance fault detection a chronological review, *Advances in Electrical and Computer Engineering* 10 (3) (2010) 114–128.
- [10] J. Li, G. Zou, W. Wang, N. Shao, B. Han, L. Wei, Low-voltage series arc fault detection based on ecmc and vb-scn, *Electric Power Systems Research* 218 (2023) 109222.
- [11] B. Wang, J. Geng, X. Dong, High-impedance fault detection based on nonlinear voltage–current characteristic profile identification, *IEEE Transactions on Smart Grid* 9 (4) (2016) 3783–3791.
- [12] Modified fft based high impedance fault detection technique considering distribution non-linear loads: Simulation and experimental data analysis, *International Journal of Electrical Power and Energy Systems* 94 (2018) 124–140.
- [13] Y. Wang, D. Sheng, H. Hu, K. Han, J. Zhou, L. Hou, A novel series arc fault detection method based on mel-frequency cepstral coefficients and fully connected neural network, *IEEE Access* 10 (2022) 97983–97994.
- [14] N. I. Elkalashy, M. Lehtonen, H. A. Darwish, M. A. Izzularab, A.-m. I. Taalab, Modeling and experimental verification of high impedance arcing fault in medium voltage networks, *IEEE Transactions on Dielectrics and Electrical Insulation* 14 (2) (2007) 375–383. doi:10.1109/TDEI.2007.344617.
- [15] A. Ghaderi, H. A. Mohammadpour, H. L. Ginn, Y.-J. Shin, High-impedance fault detection in the distribution network using the time-frequency-based algorithm, *IEEE Transactions on Power Delivery* 30 (3) (2014) 1260–1268.

- [16] H. Lala, S. Karmakar, Detection and experimental validation of high impedance arc fault in distribution system using empirical mode decomposition, *IEEE Systems Journal* 14 (3) (2020) 3494–3505.
- [17] L. Wang, H. Qiu, P. Yang, L. Mu, Arc fault detection algorithm based on variational mode decomposition and improved multi-scale fuzzy entropy, *Energies* 14 (14) (2021) 4137.
- [18] N. Qu, J. Wang, J. Liu, An arc fault detection method based on current amplitude spectrum and sparse representation, *IEEE Transactions on Instrumentation and Measurement* 68 (10) (2018) 3785–3792.
- [19] M. Wei, W. Liu, F. Shi, H. Zhang, Z. Jin, W. Chen, Distortion-controllable arc modeling for high impedance arc fault in the distribution network, *IEEE Transactions on Power Delivery* 36 (1) (2020) 52–63.
- [20] Y. Wang, F. Zhang, X. Zhang, S. Zhang, Series ac arc fault detection method based on hybrid time and frequency analysis and fully connected neural network, *IEEE Transactions on Industrial Informatics* 15 (12) (2018) 6210–6219.
- [21] M. Korda, I. Mezić, Linear predictors for nonlinear dynamical systems: Koopman operator meets model predictive control, *Automatica* 93 (2018) 149–160.
- [22] S. L. Brunton, B. W. Brunton, J. L. Proctor, E. Kaiser, J. N. Kutz, Chaos as an intermittently forced linear system, *Nature communications* 8 (1) (2017) 19.
- [23] J. Tu, C. Rowley, D. Luchtenburg, S. Brunton, J. Kutz, On dynamic mode decomposition: Theory and applications, *Journal of Computational Dynamics* 1 (11 2013). doi:10.3934/jcd.2014.1.391.
- [24] D. Dwivedi, P. K. Yemula, M. Pal, Dynamopmu: A physics informed anomaly detection, clustering and prediction method using non-linear dy-

- namics on  $\mu$ pmu measurements, *IEEE Transactions on Instrumentation and Measurement* (2023).
- [25] J. Yang, J. Zhao, J. Song, J. Wu, C. Zhao, H. Leng, A hybrid method using havok analysis and machine learning for predicting chaotic time series, *Entropy* 24 (3) (2022) 408.
- [26] R. G. Moulder, E. Martynova, S. M. Boker, Extracting nonlinear dynamics from psychological and behavioral time series through havok analysis, *Multivariate Behavioral Research* 58 (2) (2023) 441–465.
- [27] W. CIGRE, 13.01. practical application of arc physics in circuit breakers. survey of calculation methods and application guide, *Electra* 118 (1988) 63–79.
- [28] P. H. Schavemaker, L. Van der Slui, An improved mayr-type arc model based on current-zero measurements [circuit breakers], *IEEE Transactions on Power delivery* 15 (2) (2000) 580–584.
- [29] J. Guardado, S. Maximov, E. Melgoza, J. Naredo, P. Moreno, An improved arc model before current zero based on the combined mayr and cassie arc models, *IEEE Transactions on Power Delivery* 20 (1) (2005) 138–142.
- [30] S. Qian, C. A. Chou, A koopman-operator-theoretical approach for anomaly recognition and detection of multi-variate eeg system, *Biomedical Signal Processing and Control* 69 (2021) 102911.
- [31] P. K. Huynh, A. R. Setty, T. B. Le, T. Q. Le, A noise-robust koopman spectral analysis of an intermittent dynamics method for complex systems: a case study in pathophysiological processes of obstructive sleep apnea, *IIEE Transactions on Healthcare Systems Engineering* 0 (0) (2022) 1–16.
- [32] V. V. Terzija, H.-J. Koglin, On the modeling of long arc in still air and arc resistance calculation, *IEEE Transactions on Power Delivery* 19 (3) (2004) 1012–1017.

- [33] A. Gaudreau, B. Koch, Evaluation of lv and mv arc parameters, *IEEE Transactions on Power Delivery* 23 (1) (2007) 487–492.
- [34] A. Ghaderi, H. L. Ginn III, H. A. Mohammadpour, High impedance fault detection: A review, *Electric power systems research* 143 (2017) 376–388.
- [35] S. Kavaskar, N. K. Mohanty, Detection of high impedance fault in distribution networks, *Ain Shams Engineering Journal* 10 (1) (2019) 5–13.  
doi:<https://doi.org/10.1016/j.asej.2018.04.006>.  
URL <https://www.sciencedirect.com/science/article/pii/S209044791830087X>
- [36] V. Torres, J. Guardado, H. Ruiz, S. Maximov, Modeling and detection of high impedance faults, *International Journal of Electrical Power & Energy Systems* 61 (2014) 163–172. doi:<https://doi.org/10.1016/j.ijepes.2014.03.046>.  
URL <https://www.sciencedirect.com/science/article/pii/S0142061514001483>
- [37] K. Moloi, I. Davidson, High impedance fault detection protection scheme for power distribution systems, *Mathematics* 10 (22) (2022) 4298.